Biomedical Optics EXPRESS

Application of time-resolved autofluorescence to label-free in vivo optical mapping of changes in tissue matrix and metabolism associated with myocardial infarction and heart failure

João Lagarto,[1,3,*] Benjamin T. Dyer,[2,3] Clifford Talbot,[1] Markus B. Sikkel,[2] Nicholas S. Peters,[2] Paul M. W. French,[2] Alexander R. Lyon,[2,4] and Chris Dunsby[1,4]

[1] *Photonics Group, Department of Physics, Imperial College London, Prince Consort Road, London, SW7 2AZ UK*
[2] *National Heart and Lung Institute, Imperial College London, Du Cane Road, London, W12 0NN UK*
[3] *Authors contributed equally to this work*
[4] *Authors contributed equally to this work*
[*] *joao.lagarto11@imperial.ac.uk*

Abstract: We investigate the potential of an instrument combining time-resolved spectrofluorometry and diffuse reflectance spectroscopy to measure structural and metabolic changes in cardiac tissue in vivo in a 16 week post-myocardial infarction heart failure model in rats. In the scar region, we observed changes in the fluorescence signal that can be explained by increased collagen content, which is in good agreement with histology. In areas remote from the scar tissue, we measured changes in the fluorescence signal ($p < 0.001$) that cannot be explained by differences in collagen content and we attribute this to altered metabolism within the myocardium. A linear discriminant analysis algorithm was applied to the measurements to predict the tissue disease state. When we combine all measurements, our results reveal high diagnostic accuracy in the infarcted area (100%) and border zone (94.44%) as well as in remote regions from the scar (> 77%). Overall, our results demonstrate the potential of our instrument to characterize structural and metabolic changes in a failing heart in vivo without using exogenous labels.

OCIS codes: (170.3650) Lifetime-based sensing; (300.6500) Spectroscopy, time-resolved; (170.3890) Medical optics instrumentation; (170.4580) Optical diagnostics for medicine; (170.6935) Tissue characterization; (170.1610) Clinical applications.

References and links

1. L. Marcu, "Fluorescence lifetime techniques in medical applications," Ann. Biomed. Eng. **40**(2), 304–331 (2012).
2. A. P. Koretsky, L. A. Katz, and R. S. Balaban, "Determination of pyridine nucleotide fluorescence from the perfused heart using an internal standard," Am. J. Physiol. **253**(4 Pt 2), H856–H862 (1987).
3. J. Eng, R. M. Lynch, and R. S. Balaban, "Nicotinamide adenine dinucleotide fluorescence spectroscopy and imaging of isolated cardiac myocytes," Biophys. J. **55**(4), 621–630 (1989).
4. S. Huang, A. A. Heikal, and W. W. Webb, "Two-photon fluorescence spectroscopy and microscopy of NAD(P)H and flavoprotein," Biophys. J. **82**(5), 2811–2825 (2002).
5. D. Chorvat, J. Kirchnerova, M. Cagalinec, J. Smolka, A. Mateasik, and A. Chorvatova, "Spectral unmixing of flavin autofluorescence components in cardiac myocytes," Biophys. J. **89**(6), L55–L57 (2005).
6. K. Konig, K. Schenke-layland, I. Riemann, and U. A. Stock, "Multiphoton autofluorescence imaging of intratissue elastic fibers," Biomaterials **26**, 495–500 (2004).
7. Y. Ti, P. Chen, and W.-C. Lin, "In vivo characterization of myocardial infarction using fluorescence and diffuse reflectance spectroscopy," J. Biomed. Opt. **15**(3), 037009 (2010).
8. K. T. Weber, "Cardiac interstitium in health and disease: the fibrillar collagen network," J. Am. Coll. Cardiol. **13**(7), 1637–1652 (1989).

#220276 - $15.00 USD Received 6 Aug 2014; revised 17 Oct 2014; accepted 21 Oct 2014; published 7 Jan 2015

9. S. M. Weis, J. L. Emery, K. D. Becker, D. J. McBride, J. H. Omens, and A. D. McCulloch, "Myocardial Mechanics and Collagen Structure in the Osteogenesis Imperfecta Murine (oim)," Circ. Res. **87**(8), 663–669 (2000).
10. B. Chance, P. Cohen, F. Jobsis, and B. Schoener, "Intracellular oxidation-reduction states in vivo," Science **137**(3529), 499–508 (1962).
11. A. Pradhan, P. Pal, G. Durocher, L. Villeneuve, A. Balassy, F. Babai, L. Gaboury, and L. Blanchard, "Steady state and time-resolved fluorescence properties of metastatic and non-metastatic malignant cells from different species," J. Photochem. Photobiol. B **31**(3), 101–112 (1995).
12. A. Mayevsky and B. Chance, "Oxidation-reduction states of NADH in vivo: from animals to clinical use," Mitochondrion **7**(5), 330–339 (2007).
13. M. C. Skala, K. M. Riching, A. Gendron-Fitzpatrick, J. Eickhoff, K. W. Eliceiri, J. G. White, and N. Ramanujam, "In vivo multiphoton microscopy of NADH and FAD redox states, fluorescence lifetimes, and cellular morphology in precancerous epithelia," Proc. Natl. Acad. Sci. U.S.A. **104**(49), 19494–19499 (2007).
14. V. Lutz, M. Sattler, S. Gallinat, H. Wenck, R. Poertner, and F. Fischer, "Impact of collagen crosslinking on the second harmonic generation signal and the fluorescence lifetime of collagen autofluorescence," Skin Res. Technol. **18**(2), 168–179 (2012).
15. A. E. Arai, C. E. Kasserra, P. R. Territo, A. H. Gandjbakhche, and R. S. Balaban, "Myocardial oxygenation in vivo: optical spectroscopy of cytoplasmic myoglobin and mitochondrial cytochromes," Am. J. Physiol. **277**(2 Pt 2), H683–H697 (1999).
16. D. Baykut, M. M. Gebhard, H. Bölükoglu, K. Kadipasaoglu, S. Hennes, O. H. Frazier, and A. Krian, "Online detection of myocardial ischemia by near infrared spectroscopy with a fiberoptic catheter," Thorac. Cardiovasc. Surg. **49**(3), 162–166 (2001).
17. J. Swartling, S. Pålsson, P. Platonov, S. B. Olsson, and S. Andersson-Engels, "Changes in tissue optical properties due to radio-frequency ablation of myocardium," Med. Biol. Eng. Comput. **41**(4), 403–409 (2003).
18. E. Häggblad, T. Lindbergh, M. G. D. Karlsson, H. Casimir-Ahn, E. G. Salerud, and T. Strömberg, "Myocardial tissue oxygenation estimated with calibrated diffuse reflectance spectroscopy during coronary artery bypass grafting," J. Biomed. Opt. **13**(5), 054030 (2008).
19. A. Mayevsky, T. Manor, E. Pevzner, A. Deutsch, R. Etziony, N. Dekel, and A. Jaronkin, "Tissue spectroscope: a novel in vivo approach to real time monitoring of tissue vitality," J. Biomed. Opt. **9**(5), 1028–1045 (2004).
20. M. Ranji, S. Member, M. Matsubara, B. G. Leshnower, R. H. Hinmon, D. L. Jaggard, B. Chance, L. Fellow, R. C. Gorman, and J. H. Gorman, "Quantifying acute myocardial injury using ratiometric fluorometry" IEEE Biomed. Eng. **56**, 1556–1563 (2009).
21. L. Marcu, "Fluorescence lifetime in cardiovascular diagnostics," J. Biomed. Opt. **15**(1), 011106 (2010).
22. J. R. Lakowicz, *Principles of Fluorescence Spectroscopy* (Springer, 2006), Vol. 13, p. 029901.
23. M. A. Bennet, P. R. Richardson, J. Arlt, A. McCarthy, G. S. Buller, and A. C. Jones, "Optically trapped microsensors for microfluidic temperature measurement by fluorescence lifetime imaging microscopy," Lab Chip **11**(22), 3821–3828 (2011).
24. H. C. Gerritsen, R. Sanders, A. Draaijer, C. Ince, and Y. K. Levine, "Fluorescence lifetime imaging of oxygen in living cells," J. Fluoresc. **7**(1), 11–15 (1997).
25. H.-J. Lin, P. Herman, and J. R. Lakowicz, "Fluorescence lifetime-resolved pH imaging of living cells," Cytometry A **52**(2), 77–89 (2003).
26. R. Sanders, H. C. Gerritsen, A. Draaijer, P. M. Houpt, and Y. K. Levine, "Confocal fluorescence lifetime imaging of free calcium in single cells," J. Fluoresc. **4**(4), 291–294 (1994).
27. K. Carlsson and A. Liljeborg, "Confocal fluorescence microscopy using spectral and lifetime information to simultaneously record four fluorophores with high channel separation," J. Microscopy **185**, 37–46 (1997).
28. L. Marcu, M. C. Fishbein, J.-M. I. Maarek, and W. S. Grundfest, "Discrimination of Human Coronary Artery Atherosclerotic Lipid-Rich Lesions by Time-Resolved Laser-Induced Fluorescence Spectroscopy," Arterioscler. Thromb. Vasc. Biol. **21**(7), 1244–1250 (2001).
29. M. Chandra, J. Scheiman, D. Heidt, D. Simeone, B. McKenna, and M.-A. Mycek, "Probing pancreatic disease using tissue optical spectroscopy," J. Biomed. Opt. **12**(6), 060501 (2007).
30. P. A. A. De Beule, C. Dunsby, N. P. Galletly, G. W. Stamp, A. C. Chu, U. Anand, P. Anand, C. D. Benham, A. Naylor, and P. M. French, "A hyperspectral fluorescence lifetime probe for skin cancer diagnosis," Rev. Sci. Instrum. **78**(12), 123101 (2007).
31. S. Coda, A. J. Thompson, G. T. Kennedy, K. L. Roche, L. Ayaru, D. S. Bansi, G. W. Stamp, A. V. Thillainayagam, P. M. W. French, and C. Dunsby, "Fluorescence lifetime spectroscopy of tissue autofluorescence in normal and diseased colon measured ex vivo using a fiber-optic probe," Biomed. Opt. Express **5**(2), 515–538 (2014).
32. M.-A. Mycek, K. T. Schomacker, and N. S. Nishioka, "Colonic polyp differentiation using time-resolved autofluorescence spectroscopy," Gastrointest. Endosc. **48**(4), 390–394 (1998).
33. T. Glanzmann, J.-P. Ballini, H. van den Bergh, and G. Wagnières, "Time-resolved spectrofluorometer for clinical tissue characterization during endoscopy," Rev. Sci. Instrum. **70**(10), 4067 (1999).
34. J. A. Jo and L. Marcu, "Laguerre-based method for analysis of time-resolved fluorescence data: application to in-vivo characterization and diagnosis of atherosclerotic lesions," J. Biomed. Opt. **11**, 1–22 (2009).
35. A. J. Thompson, S. Coda, M. B. Sørensen, G. Kennedy, R. Patalay, U. Waitong-Brämming, P. A. De Beule, M. A. Neil, S. Andersson-Engels, N. Bendsøe, P. M. French, K. Svanberg, and C. Dunsby, "In vivo measurements

#220276 - $15.00 USD Received 6 Aug 2014; revised 17 Oct 2014; accepted 21 Oct 2014; published 7 Jan 2015

of diffuse reflectance and time-resolved autofluorescence emission spectra of basal cell carcinomas," J. Biophotonics **5**(3), 240–254 (2012).
36. A. R. Lyon, K. T. MacLeod, Y. Zhang, E. Garcia, G. K. Kanda, M. J. Lab, Y. E. Korchev, S. E. Harding, and J. Gorelik, "Loss of T-tubules and other changes to surface topography in ventricular myocytes from failing human and rat heart," Proc. Natl. Acad. Sci. U.S.A. **106**(16), 6854–6859 (2009).
37. V. O. Nikolaev, A. Moshkov, A. R. Lyon, M. Miragoli, P. Novak, H. Paur, M. J. Lohse, Y. E. Korchev, S. E. Harding, and J. Gorelik, "Beta2-adrenergic receptor redistribution in heart failure changes cAMP compartmentation," Science **327**(5973), 1653–1657 (2010).
38. A. R. Lyon, M. L. Bannister, T. Collins, E. Pearce, A. H. Sepehripour, S. S. Dubb, E. Garcia, P. O'Gara, L. Liang, E. Kohlbrenner, R. J. Hajjar, N. S. Peters, P. A. Poole-Wilson, K. T. Macleod, and S. E. Harding, "SERCA2a gene transfer decreases sarcoplasmic reticulum calcium leak and reduces ventricular arrhythmias in a model of chronic heart failure," Circ Arrhythm Electrophysiol **4**(3), 362–372 (2011).
39. R. Kumarswamy, A. R. Lyon, I. Volkmann, A. M. Mills, J. Bretthauer, A. Pahuja, C. Geers-Knörr, T. Kraft, R. J. Hajjar, K. T. Macleod, S. E. Harding, and T. Thum, "SERCA2a gene therapy restores microRNA-1 expression in heart failure via an Akt/FoxO3A-dependent pathway," Eur. Heart J. **33**(9), 1067–1075 (2012).
40. A. R. Lyon, V. O. Nikolaev, M. Miragoli, M. B. Sikkel, H. Paur, L. Benard, J.-S. Hulot, E. Kohlbrenner, R. J. Hajjar, N. S. Peters, Y. E. Korchev, K. T. Macleod, S. E. Harding, and J. Gorelik, "Plasticity of surface structures and β(2)-adrenergic receptor localization in failing ventricular cardiomyocytes during recovery from heart failure," Circ Heart Fail **5**(3), 357–365 (2012).
41. D. Cardinale, A. Colombo, G. Lamantia, N. Colombo, M. Civelli, G. De Giacomi, M. Rubino, F. Veglia, C. Fiorentini, and C. M. Cipolla, "Anthracycline-induced cardiomyopathy: clinical relevance and response to pharmacologic therapy," J. Am. Coll. Cardiol. **55**(3), 213–220 (2010).
42. D. Chorvat, Jr. and A. Chorvatova, "Spectrally resolved time-correlated single photon counting: a novel approach for characterization of endogenous fluorescence in isolated cardiac myocytes," Eur. Biophys. J. **36**(1), 73–83 (2006).
43. J. E. Phipps, N. Hatami, Z. S. Galis, J. D. Baker, M. C. Fishbein, and L. Marcu, "A fluorescence lifetime spectroscopy study of matrix metalloproteinases-2 and -9 in human atherosclerotic plaque," J. Biophotonics **4**(9), 650–658 (2011).
44. J. Park, P. Pande, S. Shrestha, F. Clubb, B. E. Applegate, and J. A. Jo, "Biochemical characterization of atherosclerotic plaques by endogenous multispectral fluorescence lifetime imaging microscopy," Atherosclerosis **220**(2), 394–401 (2012).
45. J. Venius, S. Bagdonas, E. Žurauskas, and R. Rotomskis, "Time-resolved fluorescence spectroscopy of the heart tissues," Lith. J. Phys. **51**(4), 370–376 (2011).
46. P. Whittaker, R. A. Kloner, D. R. Boughner, and J. G. Pickering, "Quantitative assessment of myocardial collagen with picrosirius red staining and circularly polarized light," Basic Res. Cardiol. **89**(5), 397–410 (1994).
47. J. Schindelin, I. Arganda-Carreras, E. Frise, V. Kaynig, M. Longair, T. Pietzsch, S. Preibisch, C. Rueden, S. Saalfeld, B. Schmid, J.-Y. Tinevez, D. J. White, V. Hartenstein, K. Eliceiri, P. Tomancak, and A. Cardona, "Fiji: an open-source platform for biological-image analysis," Nat. Methods **9**(7), 676–682 (2012).
48. G. Zonios and A. Dimou, "Modeling diffuse reflectance from semi-infinite turbid media: application to the study of skin optical properties," Opt. Express **14**(19), 8661–8674 (2006).
49. T. Lindbergh, E. Häggblad, H. Ahn, E. Göran Salerud, M. Larsson, and T. Strömberg, "Improved model for myocardial diffuse reflectance spectra by including mitochondrial cytochrome aa3, methemoglobin, and inhomogenously distributed RBC," J. Biophotonics **4**(4), 268–276 (2011).
50. C. B. Talbot, R. Patalay, I. Munro, S. Warren, F. Ratto, P. Matteini, R. Pini, H. G. Breunig, K. König, A. C. Chu, G. W. Stamp, M. A. Neil, P. M. French, and C. Dunsby, "Application of ultrafast gold luminescence to measuring the instrument response function for multispectral multiphoton fluorescence lifetime imaging," Opt. Express **19**(15), 13848–13861 (2011).
51. Y. Pu, J. Xue, W. Wang, B. Xu, Y. Gu, R. Tang, E. Ackerstaff, J. A. Koutcher, S. Achilefu, and R. R. Alfano, "Native fluorescence spectroscopy reveals spectral differences among prostate cancer cell lines with different risk levels," J. Biomed. Opt. **18**(8), 087002 (2013).
52. S. Prahl, "Optical Absorption of Hemoglobin," http://omlc.ogi.edu/spectra/hemoglobin/summary.html.
53. K. A. Schenkman, D. R. M. Arble, D. H. Burns, and E. O. Feigl, "Optical spectroscopic method for in vivo measurement of cardiac myoglobin oxygen saturation," Appl. Spectros. **53**, 332(1999).
54. E. Margoliash and N. Frohwirt, "Spectrum of horse-heart cytochrome c," Biochem. J. **71**(3), 570–572 (1959).
55. H. F. Weisman, D. E. Bush, J. A. Mannisi, and B. H. Bulkley, "Global cardiac remodeling after acute myocardial infarction: A study in the rat model," J. Am. Coll. Cardiol. **5**(6), 1355–1362 (1985).
56. L. H. Opie, P. J. Commerford, B. J. Gersh, M. A. Pfeffer, and N. England, "Controversies in cardiology" The Lancet **4**, 367 (2006).
57. N. F. Voelkel, R. A. Quaife, L. A. Leinwand, R. J. Barst, M. D. McGoon, D. R. Meldrum, J. Dupuis, C. S. Long, L. J. Rubin, F. W. Smart, Y. J. Suzuki, M. Gladwin, E. M. Denholm, and D. B. Gail, "Right ventricular function and failure: report of a National Heart, Lung, and Blood Institute working group on cellular and molecular mechanisms of right heart failure," Circulation **114**(17), 1883–1891 (2006).
58. V. Caorsi, C. Toepfer, M. B. Sikkel, A. R. Lyon, K. MacLeod, and M. A. Ferenczi, "Non-linear optical microscopy sheds light on cardiovascular disease," PLoS ONE **8**(2), e56136 (2013).

#220276 - $15.00 USD Received 6 Aug 2014; revised 17 Oct 2014; accepted 21 Oct 2014; published 7 Jan 2015

59. L. Marcu, D. Cohena, J. I. Maarek, W. S. Grundfesta, T. Development, and C. M. C. L. Angeles, "Characterization of Type I, II, III, IV, and V collagens by time-resolved laser-induced fluorescence spectroscopy," **3917**, 93–101 (2000).
60. P. Ashjian, A. Elbarbary, P. Zuk, D. A. DeUgarte, P. Benhaim, L. Marcu, and M. H. Hedrick, "Noninvasive in situ evaluation of osteogenic differentiation by time-resolved laser-induced fluorescence spectroscopy," Tissue Eng. **10**(3-4), 411–420 (2004).
61. H. B. Manning, G. T. Kennedy, D. M. Owen, D. M. Grant, A. I. Magee, M. A. A. Neil, Y. Itoh, C. Dunsby, and P. M. French, "A compact, multidimensional spectrofluorometer exploiting supercontinuum generation," J. Biophotonics **1**(6), 494–505 (2008).
62. Y. H. Li, J. C. Yue, and G. P. Cai, "Fluorescence characterization of type I collagen from normal and silicotic rats and its quenching dynamics induced by hypocrellin B," Biopolymers **42**(2), 219–226 (1997).
63. J. R. Lakowicz, H. Szmacinski, K. Nowaczyk, and M. L. Johnson, "Fluorescence lifetime imaging of free and protein-bound NADH," Proc. Natl. Acad. Sci. U.S.A. **89**(4), 1271–1275 (1992).
64. H. D. Vishwasrao, A. A. Heikal, K. A. Kasischke, and W. W. Webb, "Conformational dependence of intracellular NADH on metabolic state revealed by associated fluorescence anisotropy," J. Biol. Chem. **280**(26), 25119–25126 (2005).
65. M. C. Skala, K. M. Riching, D. K. Bird, A. Gendron-Fitzpatrick, J. Eickhoff, K. W. Eliceiri, P. J. Keely, and N. Ramanujam, "In vivo multiphoton fluorescence lifetime imaging of protein-bound and free nicotinamide adenine dinucleotide in normal and precancerous epithelia," J. Biomed. Opt. **12**(2), 024014 (2007).
66. M. S. Islam, M. Honma, T. Nakabayashi, M. Kinjo, and N. Ohta, "pH Dependence of the Fluorescence Lifetime of FAD in Solution and in Cells," Int. J. Mol. Sci. **14**(1), 1952–1963 (2013).
67. T. Doenst, T. D. Nguyen, and E. D. Abel, "Cardiac metabolism in heart failure: implications beyond ATP production," Circ. Res. **113**(6), 709–724 (2013).
68. I. Stefanon, M. Valero-Muñoz, A. A. Fernandes, R. F. Ribeiro, C. Rodríguez, M. Miana, J. Martínez-González, J. S. Spalenza, V. Lahera, P. F. Vassallo, and V. Cachofeiro, "Left and right ventricle late remodeling following myocardial infarction in rats," PLoS ONE **8**(5), e64986 (2013).
69. J. Y. Yager, R. M. Brucklacher, and R. C. Vannucci, "Cerebral oxidative metabolism and redox state during hypoxia-ischemia and early recovery in immature rats," Am. J. Physiol. **261**(4 Pt 2), H1102–H1108 (1991).
70. B. Y. M. R. Duchen and T. J. Biscoe, "Mitochondrial function in type i cells isolated from rabbit arterial," 13–31 (1992).
71. J. A. Palero, A. N. Bader, H. S. de Bruijn, A. der Ploeg van den Heuvel, H. J. C. M. Sterenborg, and H. C. Gerritsen, "In vivo monitoring of protein-bound and free NADH during ischemia by nonlinear spectral imaging microscopy," Biomed. Opt. Express **2**(5), 1030–1039 (2011).
72. S. Roth and I. Freund, "Second harmonic generation in collagen," J. Chem. Phys. **70**(4), 1637 (1979).

1. Introduction

Diseases of the myocardium such as left ventricular hypertrophy and heart failure are frequently characterized by disturbances in mitochondrial metabolism and energetic dysfunction, and alterations in extracellular matrix and interstitial fibrosis. There is growing evidence that these structural and functional abnormalities contribute to progression of contractile dysfunction and electrical instability, underpinning the progression to pump failure and malignant ventricular arrhythmias, the two leading causes of morbidity and mortality in patients with left ventricular hypertrophy and heart failure. Currently the clinical tools available to evaluate and monitor myocardial metabolism and fibrosis have a number of limitations (e.g. FDG-PET, NMR spectroscopy, LGE-CMR) including low sensitivity and suboptimal spatial resolution in addition to practical barriers including relatively high cost, limited availability and the limitations for the frequency of repeated measures in the same individual. New technologies with greater sensitivity to detect and monitor changes in myocardial metabolism and progression of fibrosis are needed, which may help guide treatment selection and stratification at an earlier stage, and also cross correlate structural and functional changes to provide new insights into the pathophysiology of myocardial disease.

Autofluorescence spectroscopy is a promising tool for characterization of biological tissues and shows potential for in vivo clinical diagnosis of diseased tissues and therefore optimization of therapeutic procedures [1]. It can exploit the photo-physical properties of endogenous fluorophores to probe the structural and functional properties of biological tissue and thus may provide label-free molecular contrast to report biochemical and metabolic information. The most common endogenous fluorophores in healthy cardiac tissue include enzyme co-factors nicotinamide adenine dinucleotide (NADH) and flavin adenine dinucleotide (FAD) [2–5], as well as extracellular matrix (ECM) components such as elastin

#220276 - $15.00 USD Received 6 Aug 2014; revised 17 Oct 2014; accepted 21 Oct 2014; published 7 Jan 2015

and collagen [6,7]. In particular, the collagen matrix in healthy myocardium consists primarily of types I (85%) and III (11%) [8,9]. Changes in the fluorescence properties of NADH and flavins can report on changes in metabolic activity [10–13] and changes in collagen fluorescence can report changes in protein cross-linking and structural changes [14].

The application of optical spectroscopy to heart disease is still very limited and only a few in vivo studies have been reported. Many of these studies utilized reflectance spectroscopy to characterize the hemodynamic state of the heart by quantification of the tissue oxygenation and hemoglobin and myoglobin concentrations [15–18]. Other studies used steady-state autofluorescence intensity or emission spectroscopy to report cardiac tissue viability and metabolic state [7,19,20]. However, intensity measurements alone are sensitive to variations in excitation efficiency, fluorophore concentration and heterogeneous sample absorption and scattering and so are difficult to compare between samples and patients [21]. Spectrally-resolved ratiometric measurements can provide quantitative readouts but their discrimination is limited by the broad overlapping fluorescence spectra of many tissue fluorophores [22].

Time-resolved fluorescence spectroscopy (TRFS) is an inherently ratiometric technique that aims to improve the specificity of fluorescence measurements by resolving the fluorescence intensity decay characteristics. Fluorescence lifetime (FL) can be sensitive to the molecular environment and therefore represents a direct approach to probe environmental parameters such as temperature [23], oxygenation [24], pH [25] or calcium concentration [26]. Furthermore, it is well suited to discriminate between fluorophores with overlapping emission spectra but different decay times [27]. TRFS has successfully been applied to tissue diagnosis in a wide range of applications, both ex vivo [28–31] and in vivo [32–35] and has shown potential for in vivo clinical diagnosis.

In this study, we report a novel approach to cardiac investigation by applying TRFS to a rat 16 week post myocardial infarction heart failure (MI-HF) model that was previously well characterized in our laboratory [36–40]. The diagnosis of heart failure traditionally rested upon demonstration of impaired systolic function of the ventricle [8], although it is clear that heart failure can occur in the absence of reduced systolic function when reported as ejection fraction. Furthermore, characteristic structural, functional, electrical, metabolic and energetic remodeling follow a myocardial injury that precedes the overt symptoms associated with more advanced impairment of systolic function. Heart failure therapies aim to "reverse remodel" the deleterious changes and their effectiveness can be increased the earlier they are instigated to prevent progression [41]. This strategy employing a contrast agent (label) free method for in vivo characterization of cardiac tissue to identify the early alterations in the failing heart would represent a useful diagnostic advance to target early therapeutic intervention.

We report the application of a compact optical fiber based instrument, which combines single point time-resolved spectrofluorometry and steady-state diffuse reflectance spectroscopy, to investigate the diagnostic potential of autofluorescence and reflectance in cardiac tissue. Although autofluorescence lifetime measurements have already been applied to studies of isolated cardiac cells [4,42] and in a number of other cardiovascular applications [21,43,44], its application to measurements of the whole heart remains limited [45]. To the best of our knowledge, this is the first *in vivo* application of TRFS to the study of cardiac tissue.

2. Materials and methods

2.1 16 week post-MI heart failure model

All work involving animal use was carried out under protocols approved and regulated under the Animals (Scientific Procedures) Act 1986 (Project Licenses PPL 70/7399 and 70/7419). Adult male Sprague-Dawley rats (Charles River UK, Ltd.) weighing 250-300g underwent proximal left anterior descending (LAD) coronary ligation to induce chronic myocardial

#220276 - $15.00 USD Received 6 Aug 2014; revised 17 Oct 2014; accepted 21 Oct 2014; published 7 Jan 2015

infarction, as previously described [36]. Five percent isoflurane anesthesia was used for induction and once the animal was intubated and ventilated, anesthesia was maintained with 2% isoflurane and opiate analgesia. Enrofloxacin (5 mg/kg) and 0.9% saline (10ml/kg) were administered preoperatively. A total of 6 animals, and their age-matched controls (AMC), were studied for *in vivo* epicardial fluorescence characteristics during a terminal procedure 16 weeks post-surgical intervention, at which time a well-characterized heart failure phenotype is established [36–40]. The animal is anesthetized by placement in an anesthetic chamber with 95%/5% O2 / isoflurane. A blunt 14G catheter is passed into the trachea under direct visualization and connected to a ventilator (Harvard Apparatus, USA). Anesthesia is maintained with 98%/2% O2 / isoflurane using tidal volume of approximately 2mL and a respiratory rate of approximately 90/min. Opiate analgesia is also given at appropriate dose for body weight. The heart and other internal organs are exposed via a laparotomy and sternotomy for spectroscopy measurements as described in section 2.5. In accordance with the reduction principle of the 3 Rs of animal research – replacement, reduction, refinement – the whole heart was explanted for cell isolation and an apical section taken for representative histology.

2.2 Histology

Cardiac tissue sampled for histology was washed in sterile PBS, fixed in 10% paraformaldehyde for 48 hours and then processed for paraffin embedding. 6μm thick sections were stained with picrosirius red (PSR) to demonstrate interstitial collagen content [46]. Whole sections were imaged using a 10x objective on a Zeiss Axio Observer inverted microscope with a fully motorized stage. Percentage interstitial fibrosis in each anatomical area of interest was quantified using Fiji image analysis software [47] by adjusting color thresholds to calculate the area of tissue positively stained with PSR.

2.3 Measurement of fluorescence emission spectra of NADH, FAD and collagen type-I

Solutions of β-NADH (N1161, Sigma-Aldrich, Germany) and FAD (F6625, Sigma-Aldrich, Germany) were prepared by diluting the respective powder in phosphate buffered saline (PBS) solution. Collagen type-I powder from rat tail was acquired from Sigma (C8897, Sigma-Aldrich, Germany) and used directly without further preparation. Measurements of the fluorescence emission spectra were carried out on a spectrofluorophotometer (RF-5301PC, Shimadzu, Japan) using 375 nm excitation light. Emission spectra were recorded from 400 to 700 nm. A 390 nm long-pass filter was placed at the entrance slit of the monochromator to prevent contamination of the fluorescence signal by the excitation light.

#220276 - $15.00 USD Received 6 Aug 2014; revised 17 Oct 2014; accepted 21 Oct 2014; published 7 Jan 2015

2.4 Instrumentation

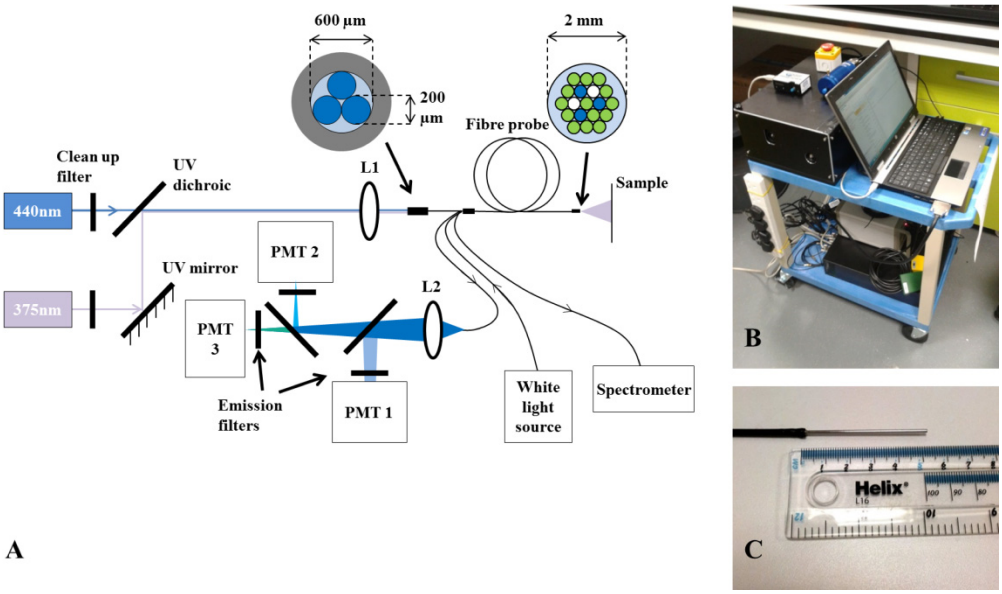

Fig. 1. (A) Experimental layout of the single point fluorescence lifetime probe system and its optical fiber configuration at the excitation (proximal) and sample (distal) ends. Optical fiber cores are colored blue for excitation fibers, white for fibers delivering white light and collecting the diffuse reflected light and green for fibers collecting the fluorescence. (B) System mounted on a portable trolley for ease of deployment in clinical settings. (C) Distal end of the fiber-optic probe.

The experiments described here were carried out using a custom-built optical fiber-based time-resolved spectrofluorometer designed to discriminate the fluorescence signals from endogenous fluorophores of interest, in particular, collagen, NADH and FAD. This system is configured as shown in Fig. 1(a). Excitation light is provided by two compact laser sources: a laser diode (LDH-P-C-375B, PicoQuant GmbH, Germany) providing 70 ps pulses at 372 nm with an average output power of 3.3 mW; and a second laser diode (LDH-P-C-440B, PicoQuant GmbH, Germany) generating 90 ps pulses at 438 nm, with 3.5 mW of average power. A single laser driver controls both lasers, allowing power control and adjustment of the repetition rate, which was set to 20 MHz. The laser beams are combined using a dichroic mirror and subsequently coupled into a custom-made optical fiber bundle (FiberTech Optica, Canada) consisting of three excitation fibers and fourteen detection fibers arranged in a hexagonal structure around the excitation fibers. There are also two extra fibers that are used for white light delivery and diffuse reflectance detection. Fluorescence light from the sample is collected by the detection fibers and directed to three spectrally resolved detection channels implemented using a set of dichroic mirrors and band-pass filters. When using 372 nm excitation, all three channels are active: the first channel collects light from 400 to 420 nm (CH1); the second channel collects light from 430 to 480 nm (CH2); the third channel accepts light from 500 to 550 nm (CH3). When using 438 nm excitation light, only the third (500-550 nm) channel is active and, for convenience, this is referred as “channel 4” (CH4) hereafter. The detection band-pass filters used are shown in Fig. 2. Each detection channel has a photon-counting photomultiplier (PMC-100-1, Becker-Hickl GmbH, Germany). The photomultipliers (PMT) are connected to a router (HRT-41, Becker-Hickl GmbH, Germany) that serializes the incoming signals for input to a time-correlated single photon counting (TCSPC) acquisition card (SPC-830, Becker-Hickl GmbH, Germany). The TCSPC system records the temporal fluorescence decay profile for each spectral channel. The instrument also comprises a white light source (HL-2000, Ocean Optics, USA) and a compact spectrometer (USB-2000 + ,

#220276 - $15.00 USD Received 6 Aug 2014; revised 17 Oct 2014; accepted 21 Oct 2014; published 7 Jan 2015

Ocean Optics, USA) for diffuse reflectance measurements. The optical setup was assembled on a 30 × 45 cm^2 breadboard (Thorlabs, USA), which was enclosed and mounted on a portable trolley for safe use and ease of deployment (see Fig. 1(b)). The system is fully controlled via a custom application written in LabVIEW (LabVIEW, National Instruments, USA).

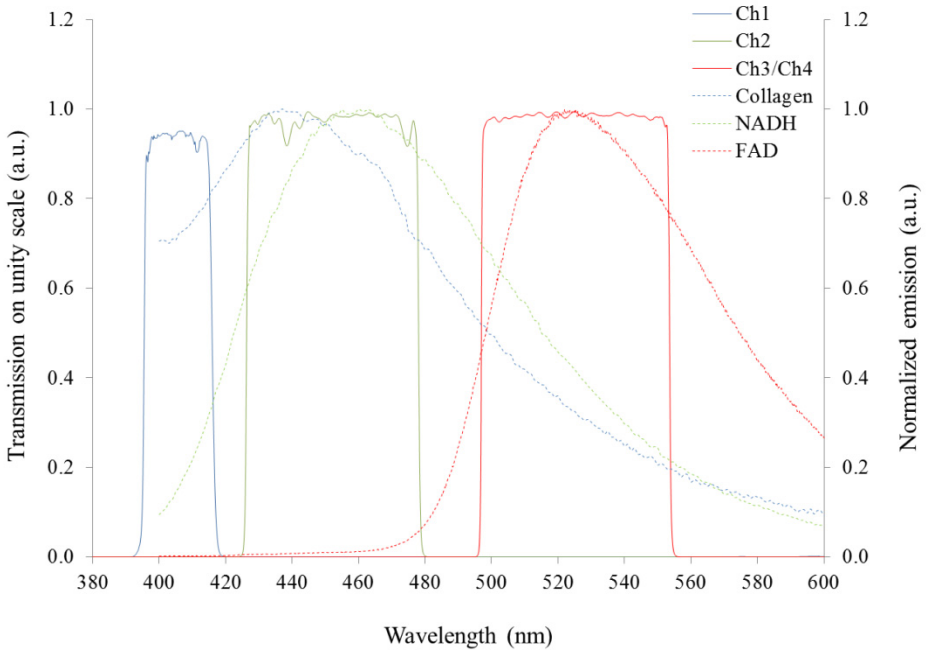

Fig. 2. Emission spectra of endogenous fluorophores of interest excited at 375 nm and plotted to show their relation to the spectral range of the detection channels of the fluorescence lifetime point probe system. Curves are normalized to their maximum amplitude. Data measured as described in section 2.3.

2.5 Data collection

In each heart, autofluorescence and diffuse reflectance data were collected from four regions of interest (ROI) (see Fig. 3): right ventricle (RV); left ventricle posterior wall (LV posterior), which represents the remaining viable myocardium in the presence of a large scar; left ventricle anterior wall/scar (LV anterior) and septum/scar border zone (border zone). In MI-HF hearts, the border zone was defined as the non-infarcted tissue at the boundary of the infarcted area – as determined visually – on the anterior wall. For pairwise comparison, we defined border zone as the septum in the AMC. All measurements were realized with the fiber optic probe in gentle contact with the epicardial surface of the heart. Due to the natural movement of the heart, the pressure of the probe tip on the surface of heart will have varied slightly during each measurement and between consecutive measurements. We therefore ensured that the fluorescence data acquisition protocol would cover multiple (typically 3-6) heart beats so that any artefacts due to the heart motion during a measurement are averaged. To further average over possible artifacts associated with the placement of the probe, we also repeated each measurement, including removal and replacement of the probe tip, at each ROI. From each ROI, we acquired 3 sets of autofluorescence and diffuse reflectance data from each of 3 random positions within the ROI, i.e. 9 measurements in total. The integration time used in a single acquisition was 1 second for UV excitation, 1 second for blue excitation and 50 milliseconds for diffuse reflectance measurements with white light illumination.

#220276 - $15.00 USD Received 6 Aug 2014; revised 17 Oct 2014; accepted 21 Oct 2014; published 7 Jan 2015

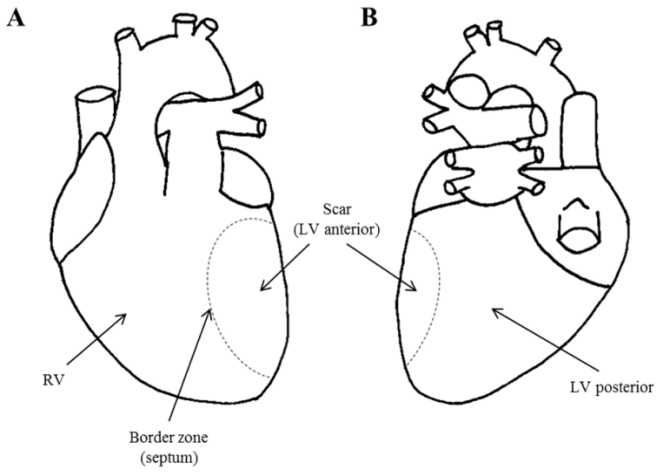

Fig. 3. Diagram of the heart illustrating regions of interest (ROI) for our measurements: (A) anterior view; (B) posterior view. "RV" - right ventricle; "LV posterior" - left ventricle posterior wall; "LV anterior (scar)" - left ventricle anterior wall; and "border zone" - scar border zone or septum.

3. Data analysis

3.1 Spectral analysis of diffuse reflectance measurements

Diffuse reflectance spectroscopy is a well-established technique that has previously been used to characterize tissue optical properties such as absorption coefficient, reduced scattering coefficient, hemoglobin and myoglobin concentrations and total blood oxygenation [15,48,49]. However, in this study we only intend to establish whether differences exist between healthy and damaged hearts. For this comparison, all acquired spectra were normalized to the signal of the diffuse reflectance from a white reference target (WS-1-SL, Labsphere, USA). All diffuse reflectance values are reported in units of absorbance, calculated as shown in Eq. (1), where A is the tissue absorbance, I is the measured spectrum and I0 is the calibrated spectrum of the white light source.

$$A(\lambda) = -\log_{10}\left(\frac{I(\lambda)}{I_0(\lambda)}\right) \tag{1}$$

3.2 Spectral analysis of fluorescence measurements

We calculated the fraction of the total autofluorescence signal in each spectral channel under UV excitation and the ratio of the autofluorescence signal between each of these channels. We excluded CH4 from ratio calculations as this is sensitive to any small day-to-day changes in fiber optic coupling efficiency and laser power differences between the 372 and 438 nm lasers. Because we aimed for the total photon counts to be approximately 1% of the laser repetition rate in each measurement, this required output power adjustment in different ROI and specimens. For each measurement, we collected a combined total of 19 lifetime and spectral parameters, as summarized in Table 3 in appendix.

3.3 Fluorescence decay analysis

Autofluorescence in biological tissue usually exhibits a complex profile due to the presence of multiple fluorophore species with overlapping spectra [1,22]. Such complex decay profiles are commonly described by a multi-exponential decay model

#220276 - $15.00 USD Received 6 Aug 2014; revised 17 Oct 2014; accepted 21 Oct 2014; published 7 Jan 2015

$$I(t) = \sum_{i=1}^{N} a_i e^{-\frac{t}{\tau}} + C \tag{2}$$

where τ_i and a_i describe the decay time and pre-exponential factor of each component in the decay and C accounts for background light. Due to the limited number of photons in each spectral channel, we chose to fit a single exponential decay model to channel 1 data and a double exponential decay model to the remaining channels. From the decay parameters in Eq. (2) applied to a double exponential decay model, we can calculate the mean lifetime as defined in Eq. (3)

$$\tau_{mean} = \beta\tau_1 + (1-\beta)\tau_2 \tag{3}$$

where β refers to the contribution of the first component to the overall decay and is calculated as shown in Eq. (4).

$$\beta = \frac{a_1\tau_1}{a_1\tau_1 + a_2\tau_2} \tag{4}$$

In order to be able to accurately fit a complex decay model to the data, it was necessary to measure the temporal instrument response function (IRF) of the system. Ideally, the measurement of the IRF includes the temporal broadening of the excitation pulse during its delivery through the excitation fiber and the broadening of the collected fluorescence through the detection fibers. We therefore measured the system response to reference fluorophores with known decay characteristics using 4′,6-Diamidino-2-phenylindole dihydrochloride (DAPI) (Sigma-Aldrich, USA) with 372 nm excitation in all detection channels and Erythrosin B (Sigma-Aldrich, USA) with 438 nm excitation. These reference dyes have lifetimes of approximately 200 ps and 90 ps, respectively, which are comparable to the pulse lengths of the lasers used.

Autofluorescence lifetime data from each detection channel was analyzed employing the non-linear least squares fitting routine from MATLAB (lsqnonlin function, R2011b, The Mathworks Inc., USA) to minimize the goodness of fit chi-square value χ^2, expressed as indicated in Eq. (5),

$$\chi^2 = \sum_{k=1}^{n} \frac{\left(I(t_k) - \mathrm{I}_{\mathrm{m}odel}(t_k)\right)^2}{I(t_k)} \tag{5}$$

where n is the number of bins in the decay, I is the measured decay at each time delay and I_{model} is the model decay function convolved with the instrument response function. The fitting model included the measured background offset and the measured after-pulsing probability of the detectors. To account for the temporal shift of the IRF with respect to the data caused by the distance between the tip of the probe and the reference dye solution, a temporal offset fit parameter was included in the fluorescence decay analysis. For all detection channels but channel 1, we extracted 4 lifetime parameters: β, τ_1, τ_2 and τ_{mean}. For channel 1, data were fitted to a single exponential decay model with lifetime τ.

3.4 Linear discriminant analysis and principal component analysis

To quantify differences between AMC and MI-HF hearts, within the corresponding ROI, we implemented a classification algorithm that is conceptually similar to the ones described in references [35,50,51], that employs principal component analysis (PCA) for feature selection followed by linear discriminant analysis (LDA) on the 5 most significant principal components (PC), using a ‘leave-one-out’ cross-validation approach that allows for each measurement to be classified as either AMC or MI-HF. A key point in our approach is that we focused on finding differences between equivalent regions of healthy and diseased hearts,

#220276 - $15.00 USD Received 6 Aug 2014; revised 17 Oct 2014; accepted 21 Oct 2014; published 7 Jan 2015

rather than distinguishing between different regions within the same heart. This is because, in a potential cardiovascular procedure guided by fluoroscopy, the position of the probe within the heart would be known but not the condition of different regions of the heart. As a first step to generate a diagnostic algorithm to discriminate healthy and diseased heart in specific ROI, each individual point measurement was used in this analysis providing a total of 54 measurements per condition (9 measurements per ROI in 6 specimens). Receiver operator characteristic (ROC) curves were generated from the scores of each classification. The performance of each classifier was measured by the area under the ROC curve (AUC).

3.5 Statistical analysis

Data results are expressed as mean ± standard deviation (SD). Statistical analysis of different groups was computed using a two-tailed Student t-test. A p-value < 0.05 was considered to be significant. p-values for all ROI are presented in Table 4 in appendix. The discriminating power of each parameter for all ROI was calculated using the Cohen's d coefficient (see Table 5 in appendix).

4. Results

4.1 16 week post MI-HF model

Cardiac occlusion of the left anterior descending artery (LAD) produced a large transmural MI and thus formation of scar tissue in the anterior wall of the left ventricle in all specimens (see Fig. 4). Compensatory hypertrophy of the remaining myocardium was confirmed by a significant increase ($p < 0.05$, $n = 6$) in heart to body weight ratio in MI-HF animals (3.40 ± 0.60 g/kg) compared to AMC animals (2.84 ± 0.45 g/kg), in agreement with previous studies of this model [36]. Collagen content of the heart significantly increased in MI-HF animals compared to AMC (see Table 1 and Fig. 4).

Table 1. Collagen content calculated from representative histology images. Statistical analysis between AMC and MI hearts was computed using a two-tailed Student t-test (n = 3).

	Collagen content assessed by PSR staining (%)		
	AMC	MI-HF	p-value
RV	4.50 ± 1.69	22.87 ± 4.17	0.0021
LV posterior	6.53 ± 1.98	35.49 ± 9.09	0.0057
Border zone	4.65 ± 0.73	28.30 ± 1.30	< 0.0001
LV anterior	2.64 ± 0.17	74.19 ± 5.02	< 0.0001

#220276 - $15.00 USD Received 6 Aug 2014; revised 17 Oct 2014; accepted 21 Oct 2014; published 7 Jan 2015

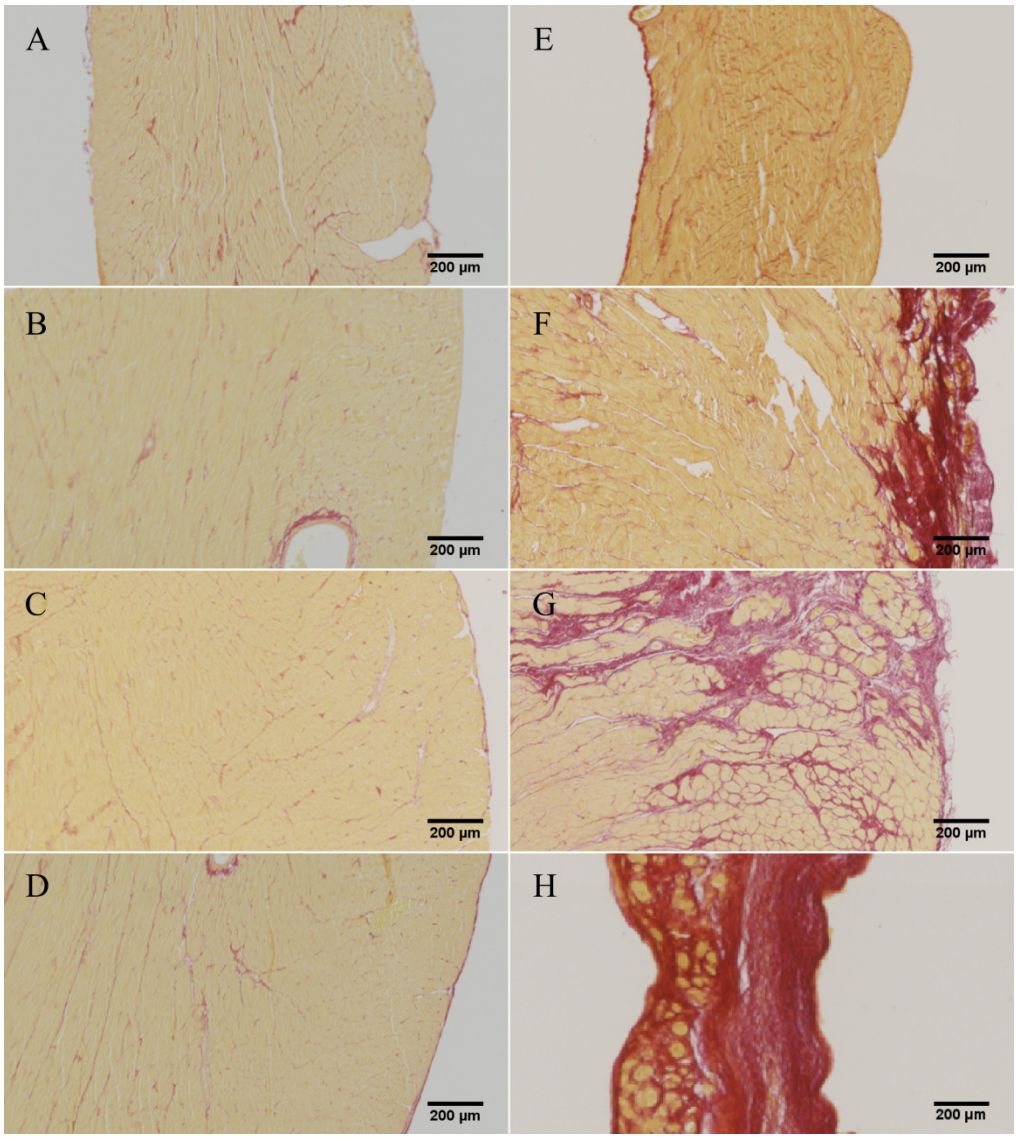

Fig. 4. Representative histology images from of AMC (left column) and MI-HF (right column) hearts. (A, E) RV; (B, F) LV posterior; (C, G) Border zone; (D, H) LV anterior

4.2 Diffuse reflectance measurements

Figure 5 presents the diffuse reflectance data for all ROI, indicating the tissue absorbance spectral profiles for AMC and MI-HF hearts, calculated as described in section 3.1. The data show an overall decrease in absorbance in MI-HF hearts, for all ROI. In AMC hearts, the maximum absorption peak at ~550 nm is consistent with the presence of cytochrome c. There is also a shoulder at ~580 nm, which can be attributed to the presence of the oxygenated forms of hemoglobin and myoglobin in the tissue, as expected in healthy AMC hearts (see Figs. 5 and 6). This feature is most pronounced in the RV, where there is a well-defined peak at ~580 nm. In MI-HF hearts, differences in the diffuse reflectance spectra were observed for infarcted (LV anterior) compared to non-infarcted (RV and LV posterior) regions. In scar tissue (LV anterior in MI hearts), the diffuse reflectance spectrum shows hallmark oxyhemoglobin/oxymyoglobin absorption features at ~540 and ~580 nm. We note that the

#220276 - $15.00 USD Received 6 Aug 2014; revised 17 Oct 2014; accepted 21 Oct 2014; published 7 Jan 2015

cytochrome c absorption peak is no longer visible in the mean spectrum for scar tissue, which is consistent with the low concentration of mitochondria expected owing to cell loss and replacement with scar. In regions remote to the MI, we observe a single peak in the 500 – 600 nm band at ~550 nm consistent with cytochrome c accompanied by a smooth shoulder at ~580 nm consistent with oxyhemoglobin/oxymyoglobin.

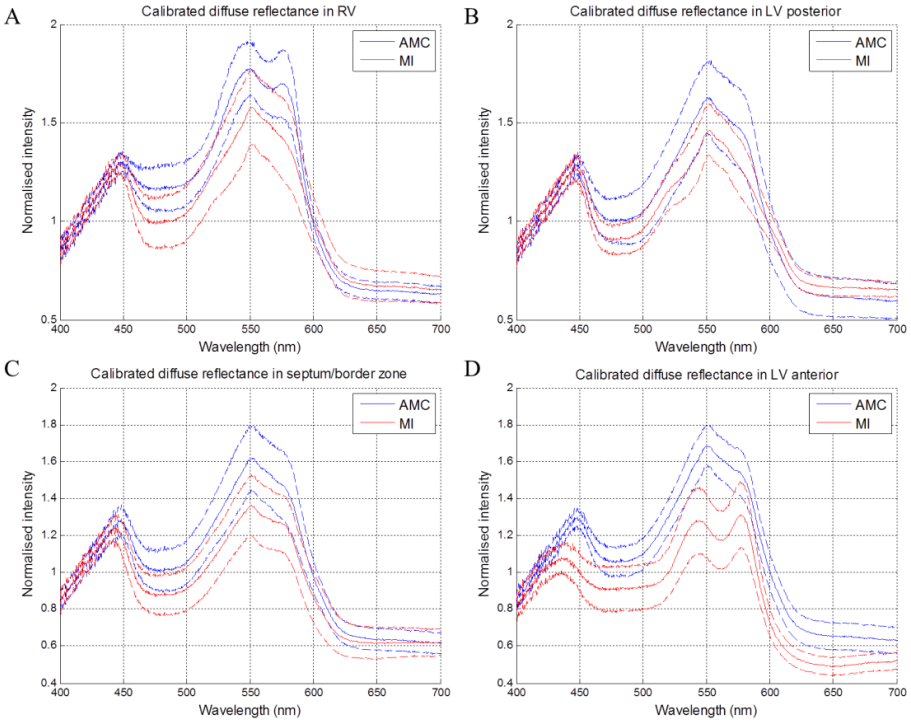

Fig. 5. Diffuse reflectance spectra in (a) RV, (b) LV posterior, (c) Border zone, (d) LV anterior. Dashed lines indicate +/– 1 SD.

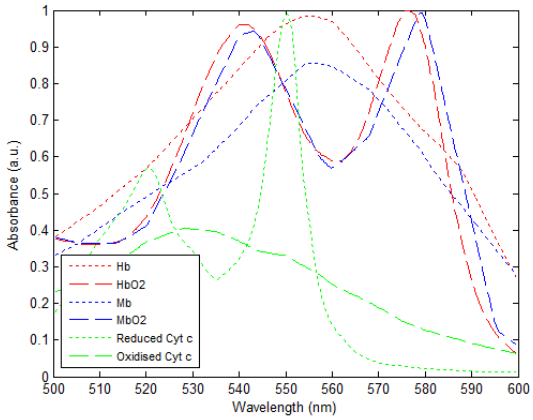

Fig. 6. Absorbance spectra of key chromophores in cardiac tissue. The absorbance curves for human Hb and HbO_2 were obtained from [52]. The absorbance curves for oxidized and reduced horse cytochrome C were obtained from [54]. The absorbance curves for horse Mb and MbO_2 were obtained from [53]. The Hb and HbO_2, Mb and MbO_2 and reduced and oxidized cytochrome c pairs of curves were scaled in proportion with the largest of each curve being normalized to 1.

#220276 - $15.00 USD Received 6 Aug 2014; revised 17 Oct 2014; accepted 21 Oct 2014; published 7 Jan 2015

4.3 Autofluorescence spectral measurements

Figure 7 shows the relative autofluorescence in each spectral channel for UV excitation by ROI (top row) and wavelength (bottom row). The results indicate an increased contribution of channel 1 to the total fluorescence signal in MI-HF hearts in all regions. This increase is most significant in LV anterior where the scar tissue was formed. Our histology (see Table 1 and Fig. 4) and previous histology [36] of this model has shown an increase in collagen type I in the scar, which, given its fluorescence emission spectrum (see Fig. 2), is consistent with the increase in fluorescence that we see in this channel. The increase in channel 1 contribution in sites remote to the MI, such as RV or LV posterior, also suggests an increase in collagen contribution in these regions, which is consistent with histology results and previous observations [7,36]. We observe an increase in the relative contribution of channel 2 in all regions, which is again consistent with an increase in collagen type I and its emission spectrum (see Fig. 2). As the total relative fluorescence signal must sum to one by definition, then the relative contribution of channel 3 to the total fluorescence signal therefore decreases for MI in all regions. The increase in collagen type I fluorescence is also apparent in the bottom row of Fig. 7 as a shift in the fluorescence emission towards shorter wavelengths for all ROI and this is most pronounced for LV anterior.

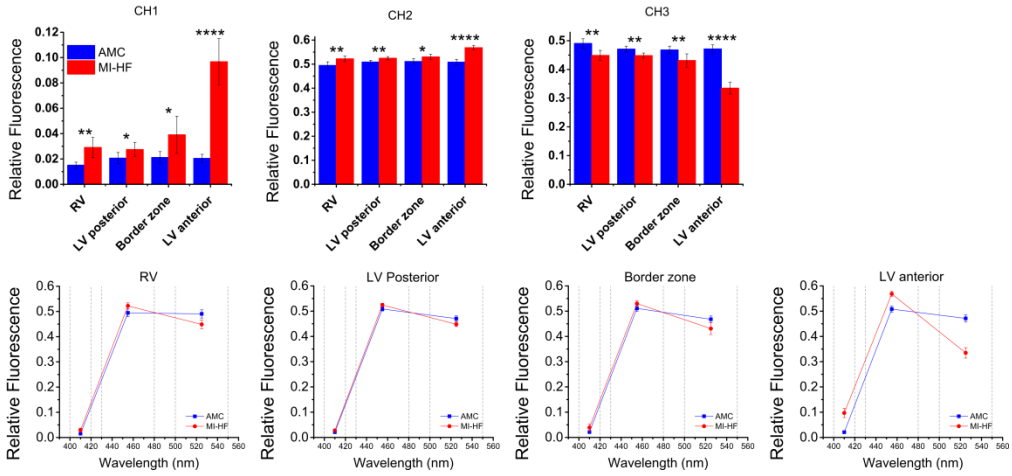

Fig. 7. Relative contribution for each spectral detection channel for AMC and MI hearts, displayed by ROI (top row) and channel center wavelength (bottom row). Dashed lines in bottom row graphs identify the spectral range of each detection channel of the FL point probe system.

4.4 Autofluorescence lifetime measurements

Results of the autofluorescence lifetime data are plotted in Fig. 8. This data shows that MI-HF scar tissue (LV anterior) yields a longer mean autofluorescence lifetime compared to healthy LV myocardium in all detection channels. The increase in mean fluorescence lifetime in the LV anterior of MI-HF hearts is also reflected in all spectral channels in both the short (τ_1) and long (τ_2) decay components and as a decrease in the relative contribution of the short decay component (β). Changes in NADH or FAD fluorescence lifetimes may also be contributing to changes in the mean fluorescence lifetime but this is challenging to quantify in the presence of the large increase in collagen autofluorescence in the infarct scar (see Table 1). Statistically significant increases in mean fluorescence lifetime are also seen in all spectral channels for the border zone (see Table 4 in appendix), which we again attribute to an increase in type-I collagen in this region. In remotes sites from scar tissue, i.e. RV and LV posterior, we also observe statistically significant differences in decay profiles of channels 3 and 4. Particularly in channel 4, we see decreases in both τ_1 and β for both regions in MI-HF compared to AMC

#220276 - $15.00 USD Received 6 Aug 2014; revised 17 Oct 2014; accepted 21 Oct 2014; published 7 Jan 2015

(Fig. 8 bottom row), which we believe cannot be explained by increases in collagen type-I concentration but might be explained by alterations in tissue metabolism in these regions.

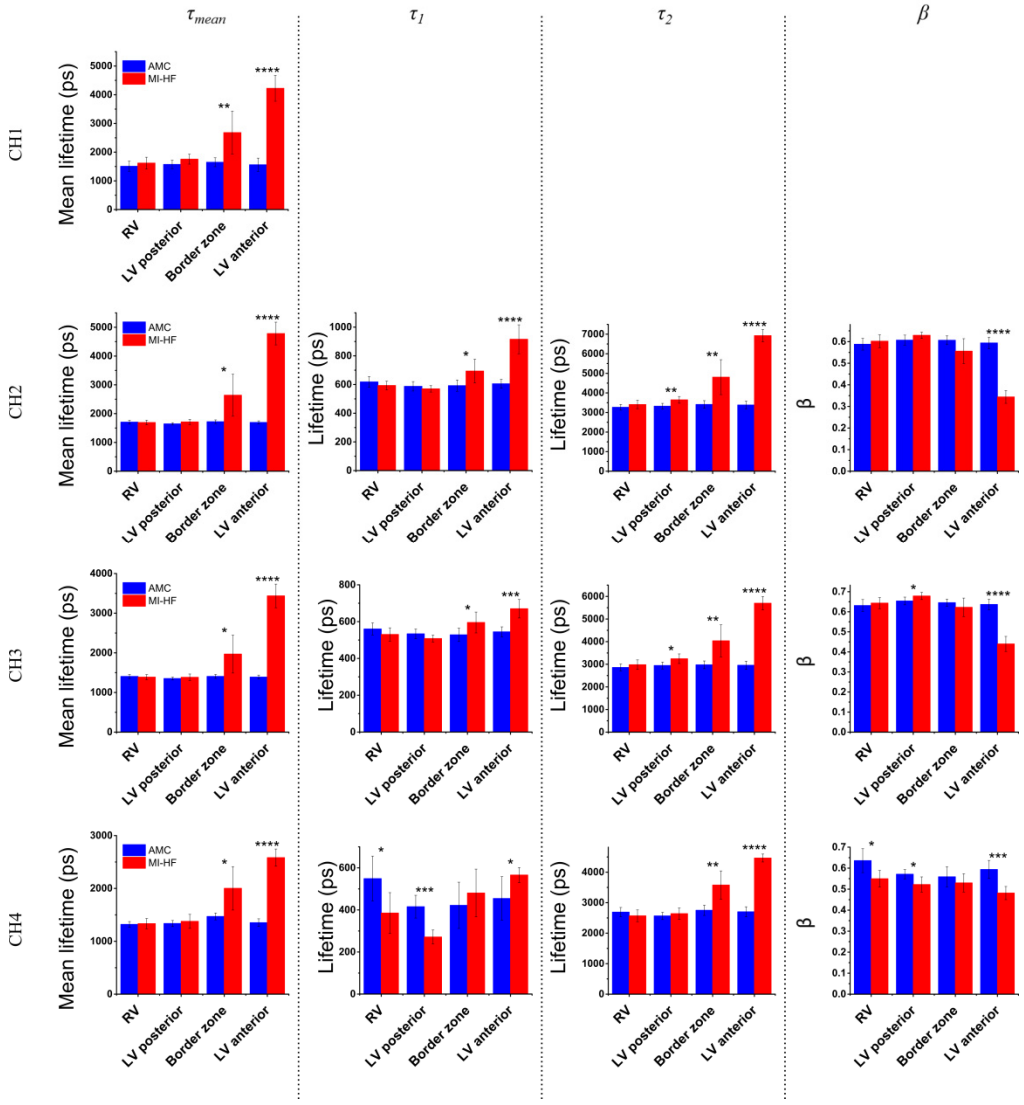

Fig. 8. Autofluorescence lifetime parameters for each spectral channel, displayed by ROI.

#220276 - $15.00 USD Received 6 Aug 2014; revised 17 Oct 2014; accepted 21 Oct 2014; published 7 Jan 2015

4.5 Discriminant analysis

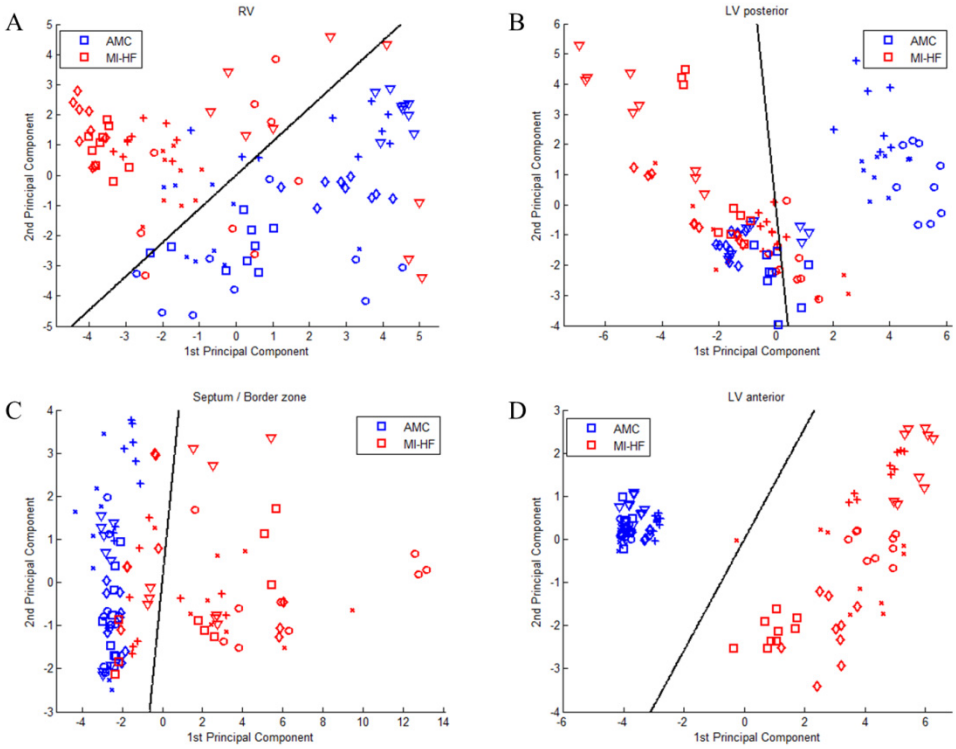

Fig. 9. Results from PCA of all spectroscopic parameters for each ROI shown as scatter plots of the scores of the first two PC for each ROI: a) RV, b) LV posterior, c) border zone and d) LV anterior. Different markers in the scatter plot identify data obtained from different specimens. Black lines show the decision lines produced by LDA analysis.

In order to illustrate the capability of our system to discriminate between healthy and infarcted hearts in each ROI, we employed PCA followed by LDA as described in section 3.4. For purposes of comparison between methods, we applied the classification algorithm separately to the following groups: diffuse reflectance; fluorescence intensity; all fluorescence data (both lifetime and intensity); diffuse reflectance and fluorescence intensity; diffuse reflectance and all fluorescence data. Figure 9 shows the scores of the first two PC for each ROI using all fluorescence parameters and Table 2 summarizes the results of the discrimination algorithm applied to all groups of measurements. Classification results show that all methods are well-suited to discriminate between healthy and diseased hearts in scar tissue (LV anterior), where the AUC values calculated from ROC curves are close to 1 for all methods, and sensitivity and specificity range from 91 to 100% and 96 to 100%, respectively, demonstrating an excellent classification performance. In regions remote to the MI, i.e. RV and LV posterior, combined diffuse reflectance and fluorescence intensity parameters achieve the best classification, with measured AUC of 0.9886 and 0.8375, respectively. Particularly in the RV, sensitivity and specificity values are high (93 and 100%, respectively) for this method. It is also relevant to observe that for LV posterior the classification is poor in comparison to other regions, thus sensitivity and specificity in this region are generally lower (76 to 87% and 61 to 71%, respectively). In the border zone, the classification is more accurate when all fluorescence parameters (lifetime and intensity) are used - either in combination with diffuse reflectance (AUC = 0.9610) or alone (AUC = 0.9599) – in comparison to steady-state methods alone, i.e. diffuse reflectance or fluorescence intensity.

#220276 - $15.00 USD Received 6 Aug 2014; revised 17 Oct 2014; accepted 21 Oct 2014; published 7 Jan 2015

Table 2. Results of the PCA/LDA discrimination algorithm applied for each ROI using fluorescence and diffuse reflectance parameters and combinations of these parameters.

		RV	LV posterior	Border zone	LV anterior
Diffuse reflectance	Variance in data (%)	97.58	98.33	98.81	98.76
	Sensitivity (%)	86.67	80.00	82.22	100.00
	Specificity (%)	75.56	64.44	80.00	97.78
	Diagnostic accuracy (%)	81.11	72.22	81.11	98.89
	AUC	0.8993	0.8247	0.8978	0.9995
Fluorescence intensity	Variance in data (%)	100.00	100.00	100.00	100.00
	Sensitivity (%)	88.89	87.04	75.93	90.74
	Specificity (%)	92.59	61.11	100.00	100.00
	Diagnostic accuracy (%)	90.74	74.07	87.96	95.37
	AUC	0.9556	0.8169	0.9009	0.9966
Fluorescence data (lifetime + intensity)	Variance in data (%)	89.31	89.77	95.57	97.47
	Sensitivity (%)	92.59	75.93	87.04	98.15
	Specificity (%)	92.59	66.67	100.00	100.00
	Diagnostic accuracy (%)	92.59	71.30	93.52	99.08
	AUC	0.9722	0.8261	0.9599	1.0000
Diffuse reflectance + Fluorescence intensity	Variance in data (%)	90.80	91.50	92.74	95.32
	Sensitivity (%)	93.33	84.44	88.89	100.00
	Specificity (%)	100.00	68.89	82.22	95.56
	Diagnostic accuracy (%)	96.67	76.67	85.56	97.78
	AUC	0.9886	0.8375	0.9235	1.0000
Diffuse reflectance + Fluorescence data (lifetime + intensity)	Variance in data (%)	90.07	90.90	92.27	95.12
	Sensitivity (%)	88.89	84.44	91.11	100.00
	Specificity (%)	95.56	71.11	97.78	100.00
	Diagnostic accuracy (%)	92.22	77.78	94.44	100.00
	AUC	0.9768	0.8351	0.9610	1.0000

5. Discussion

In this work we have described the application of a compact instrument combining time-resolved spectrofluorometry and diffuse reflectance spectroscopy to explore the potential of these label-free optical readouts in cardiac diagnosis using a rat 16-week MI heart failure model. Due to absorption and scattering of both the excitation light and emitted fluorescence, our instrument is most sensitive to fluorescence emitted near the surface of the heart, which can be a disadvantage in disease processes that vary with depth in the myocardium. However, it is known that myocardial infarction causes global alterations to the heart [55,56] and thus measurements from the epicardial surface of the heart represent a potential approach to probe its functional and structural state. In the future, incorporation of the fiber optic probe into cardiac catheters would facilitate these measurements from the endocardial surface during a minimally-invasive procedure. In addition, alternative probe geometries, e.g. with a different separation between illumination and detection fibers, could be investigated to adjust the depth probed.

One of the major challenges in studies of cardiac tissue using autofluorescence or diffuse reflectance spectroscopy in vivo is related to the movement of the beating heart. The changing pressure between the probe and the heart surface will affect the blood content of the tissue in contact with the probe tip and this will influence the optical absorption. We chose a fluorescence measurement protocol with a duration spanning several cardiac cycles in order to average this effect. In addition, we performed three repeat measurements at each spatial location to achieve an average over multiple applications of the probe tip to the tissue surface.

#220276 - $15.00 USD Received 6 Aug 2014; revised 17 Oct 2014; accepted 21 Oct 2014; published 7 Jan 2015

Changes in the optical absorption caused by the mean pressure of the probe tip will influence the measured fluorescence intensity and diffuse reflectance spectrum most strongly. Ratios of the fluorescence signal between different spectral detection channels will also be affected due to the change in absorption between channels. The fluorescence lifetime data was acquired over a relatively narrow spectral band and is inherently ratiometric. Therefore, while the pressure of the probe tip may influence the mean depth that is probed, it should not greatly influence the fluorescence decay recorded provided that the tissue structure is homogenous over the volume probed. Overall, we achieved relatively small standard deviations on the fluorescence lifetime parameters obtained from AMC hearts which indicates that any variation in lifetime caused by variations in probe pressure is small.

The diffuse reflectance spectrum is highly dependent on the absorption spectra of tissue chromophores. In cardiac tissue, the dominant chromophores are myoglobin, which is highly abundant in muscular tissue, and hemoglobin, which is present in red blood cells and is responsible for carrying oxygen to the cells. Myoglobin and hemoglobin exhibit similar absorption spectra (see Fig. 6) that are highly dependent on the tissue oxygenation [15,18]. In the presence of oxygen, the absorption spectrum of hemoglobin presents a double peak profile, with local maxima at ~540 nm and ~576 nm, as shown in Fig. 6. In contrast, in the absence of oxygen it exhibits a broader spectral profile with a single maximum peak at ~555 nm. Reduced and oxidized myoglobin present similar spectra to hemoglobin with slightly red-shifted absorption peaks. Other chromophores also contribute to the absorption spectra of heart tissue, such as mitochondrial cytochromes and cytochrome c in particular [15,51]. These play an important role in the regulation of the mitochondrial respiratory chain and therefore can provide readouts of the metabolic activity. The absorption spectrum of reduced cytochrome c has a well-defined peak at ~550 nm (see Fig. 6).

Our diffuse reflectance data is in general agreement with previous studies [7,15]. We observed a decrease of absorption in MI relative to AMC hearts, which we attribute to reduced blood content and, as consequence, decrease in hemoglobin and myoglobin concentrations in the tissue. Our data also suggests high levels of tissue oxygenation in the scar tissue. The presence of this double peak profile in scar in the heart from 2 weeks post MI was previously reported by others [7], which they attributed to some recovery of tissue oxygenation. In our model the scar tissue is very thin (~700 μm) and so an alternative explanation may be that these peaks arise due to absorption of light by oxygenated blood within the LV cavity. A similar effect appears to be occurring for measurements of the RV in AMC hearts, although in this case, because healthy RV is metabolically more active than scar tissue, the signal also reflects the contribution of mitochondrial cytochromes, in particular cytochrome c, of which the reduced form has a strong absorption peak at around 550 nm (see Fig. 6). This high level of oxygenation is not observed in the RV in MI-HF hearts, which is consistent with the previously described [57] thickening of the RV wall in MI, as consequence of the remodeling process. In LV posterior and border zone in AMC hearts, we observed a single peak profile at ~550 nm - consistent with the presence of reduced cytochrome c - accompanied by a smooth shoulder at ~580 nm that reveals the contribution to the spectra of oxygenated hemoglobin and myoglobin. This shoulder is not as evident in LV posterior in MI hearts, which may be the result of the decrease in tissue oxygenation as consequence of the reduced blood content. Future work will involve the measurement of these optical properties with the aim of developing a model of light propagation in cardiac tissue. This could also include depth resolved diffuse reflectance studies with varying illumination and detection fiber separations in order to probe the complex nature of the cardiac signal.

Our instrument recorded the autofluorescence emission into three spectral emission channels. For 372 nm excitation, the relative signal in these three channels is in agreement with the fluorescence emission spectra acquired by others [7]. In their work, Ti et al. measured the autofluorescence spectra - excited at 337 nm - of infarcted and non-infarcted regions at weeks 1 to 4 after the MI induction surgery. They observed a general increase in

#220276 - $15.00 USD Received 6 Aug 2014; revised 17 Oct 2014; accepted 21 Oct 2014; published 7 Jan 2015

autofluorescence intensity at week 1. Collagen-induced fluorescence was only visible 2 weeks post-MI with a pronounced emission peak at ~400 nm, which was also present at 4 weeks. In our model, we observe an increase in the relative fluorescence in channel 1, which suggests collagen proliferation not only in the infarction region (LV anterior) but also in sites remote to the MI reflecting interstitial fibrosis (Fig. 7), in agreement with previously published data on this model [58]. If we use the relative contribution of channel 1 to the total fluorescence signal as a quantitative measure of collagen content, we obtain a mean relative increase in collagen concentration of 93.0% in RV, 32.7% in LV posterior, 84.5% in border zone and 372% in LV anterior, which is positively correlated with qualitative observations of the histology data ($r = 0.9844$, $p < 0.05$). This result demonstrates the sensitivity of our instrument to structural changes in cardiac tissue, both in infarcted and non-infarcted remodeled regions.

We also observed an increase in the mean autofluorescence lifetime in scar tissue in all spectral channels. We believe this result can be explained by an increase in autofluorescence from collagen type-I when considering its broad emission spectrum (see Fig. 2) and its previously reported longer fluorescence lifetime. Previous studies of collagen fluorescence lifetime [59,60] have demonstrated that collagen decay characteristics are highly dependent not only of the excitation and emission spectra but also of the source of collagen itself. Using a previously described instrument [61] with excitation light at 375 nm, we have measured the fluorescence lifetime of collagen type-I from rat tail at the three emission wavelengths of interest - 410 nm, 455 nm and 525 nm - which correspond to the channel center wavelength of the single-point time-resolved spectrofluorometer used for this study. For these emission wavelengths we extracted mean lifetimes of 6.1, 5.8 and 5.9 ns, respectively. These results are within the range of what has been previously reported by others [59,60,62] and show that collagen yields a longer fluorescence lifetime compared to free and protein-bound NADH (0.4-0.5 ns and 1.0-3.0 ns respectively [63–65]) and FAD (3.0 ns to 0.3 ns respectively [65,66]). A smaller increase in mean fluorescence lifetime in MI-HF border zone relative to infarct is observed, which is consistent with a smaller rise in collagen content in this region compared to the main infarct scar.

We aimed to measure changes in the NADH and FAD fluorescence lifetimes for all regions of the heart due to changes in tissue metabolism. However, their emission spectra overlap strongly with the broad emission spectrum of collagen type-I and it is challenging to quantify changes in NADH and FAD lifetime in tissue due to significant changes in collagen concentration and the corresponding changes in fluorescence lifetime. Based on previous work by others [64], we would expect to measure a decreased fluorescence lifetime from NADH in poorly oxygenated tissue, such as scar. However, the considerable increase in collagen and its longer fluorescence lifetime, along with extensive cellular loss, masks any change in NADH lifetime in the scar region. In regions that are remote from the scar, where the absolute increase in collagen is less pronounced, e.g. LV posterior and RV, it is reasonable to attribute the changes in fluorescence lifetime to changes in the fluorescence properties of intracellular fluorophores due to changes in energetics that are seen in heart failure. In particular, we see a statistically significant decrease in the short lifetime component τ_1 excited at 438 nm in both RV and LV posterior viable myocardium in MI compared to AMC ($p < 0.05$ and $p < 0.001$, respectively). We expect the fluorescence signal in this channel to be dominated by FAD autofluorescence and the short lifetime component has previously been linked to protein-bound FAD [13]. Given the long fluorescence lifetime of collagen compared to NADH and FAD, we do not see how these changes can be attributed to additional collagen in the MI heart. We therefore attribute them to tissue metabolic remodeling in the posterior wall of the LV MI heart that causes a change in autofluorescence signal due to the increased work load and altered metabolic state. This concept of alteration in the energetic state in the failing heart is well-established [67,68].

Changes in the metabolic state of tissue are also known to affect the optical redox ratio of NADH to FAD fluorescence in biological tissues [13,69–71]. In our instrument, the redox

#220276 - $15.00 USD Received 6 Aug 2014; revised 17 Oct 2014; accepted 21 Oct 2014; published 7 Jan 2015

ratio might, in principle, be estimated from the ratio of the fluorescence intensities measured in channels 2 and 3, which, in healthy cardiac tissue, is equivalent to the ratio [NADH]/(α[NADH] + β[FAD]), where α and β represent the relative contributions of NADH and FAD respectively to channel 3 intensity under 372 nm excitation. However, although we were expecting to observe changes in the redox ratio in MI-HF hearts due to energetic alterations, as discussed above, the autofluorescence signals of channels 2 and 3 are "contaminated" by collagen type I autofluorescence, making it challenging to discern the origin of changes in the measurement, which could be structural or metabolic alterations of the tissue. This emphasizes the importance of any information concerning metabolic alterations in the tissue that can be provided by fluorescence decay measurements that are not masked by structural changes, e.g. associated with collagen. Our measurements of the short lifetime component associated with FAD autofluorescence, which has been previously associated with the protein-bound state of the molecule, are not confounded by changes in collagen autofluorescence and appear to indicate changes in the energetic state of the tissue. To summarize, our results suggest that the single-point time-resolved spectrofluorometer can read out structural and energetic alterations in the tissue. Structural alterations associated with fibrosis were indicated by both steady-state autofluorescence parameters (i.e. shift in the autofluorescence emission spectra towards shorter wavelengths) and time-resolved parameters (i.e. increase in the mean autofluorescence lifetime in all spectral channels). We note that this increase in collagen could also be detected using other approaches such as SHG microscopy [72]. However, the change in the FAD short component lifetime, which we provisionally associate with altered metabolism in the failing heart, provides information that is only available through time-resolved autofluorescence data.

To validate the potential of our instrument to distinguish healthy from diseased cardiac tissue, we implemented a discrimination algorithm, employing PCA followed by LDA, on a leave-one-out cross-validation approach. For consistency between methods, the five most significant PC were used as predictor variables in the discrimination matrix for all methods and for all combinations of methods. Our results, presented in Table 2, show that all methods provide excellent discriminant capabilities when applied directly to the infarcted region. This is expected as in this model the scar is completed and mature and could easily be determined visually due to its coloration. However, it is interesting to note that the best discriminant parameters in LV anterior - calculated through the Cohen's d coefficient (see Table 5 in appendix) - are lifetime related parameters, which is consistent with the higher diagnostic accuracy calculated for classifications that include these parameters. In the border zone region, the accuracy of the classification decreased compared to that achieved for classification of scar. Our results show that steady-state methods alone provide a lower accuracy than when combined with time-resolved parameters. Classification results for LV anterior and border zone suggest that lifetime parameters are more sensitive to increase in collagen content - and therefore structural changes in the tissue - for the excitation and detection wavelengths used in this study. In sites remote to the MI, our results show that intensity based parameters provide better discrimination between healthy and diseased myocardium compared to lifetime based parameters. This is particularly evident in RV (see Table 5 in appendix) and explains the classification results in this ROI, which show that fluorescence intensity parameters in combination with diffuse reflectance provide the most accurate tissue state classification. In LV posterior myocardium, it is interesting to observe that the best discrimination parameter is the short lifetime component extracted from the channel 4 fluorescence decay. As discussed above, we believe that the observed change in this parameter does not reflect an increase in collagen content, but may explain the energetic impairment in the myocardium in post-MI heart failure. It is also relevant to point out that the best discriminant parameters given by the Cohen's d statistics in this ROI occur in channels 2, 3 and 4 - which include the emission wavelengths of NADH and FAD - and can also be associated to alterations in energetic state. As collagen proliferation is still observed through

#220276 - $15.00 USD Received 6 Aug 2014; revised 17 Oct 2014; accepted 21 Oct 2014; published 7 Jan 2015

histology, we believe that the autofluorescence signal collected in this anatomical area is a result of both structural and metabolic changes.

6. Conclusions

We have presented an exploration of in vivo time-resolved spectrofluorometry and diffuse reflectance spectroscopy with a view to developing a new cardiac diagnostic tool. We have demonstrated the potential of our instrument to report structural and metabolic changes in cardiac tissue in a 16 week post-MI heart failure model in rats, not only in the anatomical area of infarction but, more excitingly, also in remodeled myocardium remote from the scar where we report, for the first time, changes in the autofluorescence signal that we provisionally attribute to metabolic alterations within the myocardium. Using a PCA-based discrimination algorithm we were also able to accurately distinguish healthy from diseased myocardium, even in sites remote to the infarction where changes in tissue properties are more subtle. Future work will characterize the autofluorescence lifetime signature at earlier time-points during the development of heart failure following MI, particularly before extensive collagen proliferation occurs. Once the autofluorescence signatures that accompany the structural, functional and metabolic aberrations in other cardiac disease states have been further characterized, this approach could be applied either during open-chest procedures or via incorporation of fiber optic probe into coronary angiography or electrophysiology catheters. Catheter-based autofluorescence measurements have the potential to be relatively low cost compared to PET or functional MRI and could be performed without the need for contrast agents, e.g. during angioscopy or between catheter-based ablation procedures, to provide feedback to the clinician. Autofluorescence measurements also have the potential to be used during open-chest surgery while the patient is still connected to a heart and lung machine.

Appendix

Table 3. List of spectroscopic parameters extracted from a single fluorescence lifetime measurement

Channel	Index	Description
Channel 1	τ	Fluorescence lifetime
Channel 2	τ_{mean}	Weighted mean fluorescence lifetime
	τ_1	Short lifetime component
	τ_2	Long lifetime component
	β	Contribution of the first component
Channel 3	τ_{mean}	Weighted mean fluorescence lifetime
	τ_1	Short lifetime component
	τ_2	Long lifetime component
	β	Contribution of the first component
Channel 4	τ_{mean}	Weighted mean fluorescence lifetime
	τ_1	Short lifetime component
	τ_2	Long lifetime component
	β	Contribution of the first component
	CH1 R	Relative fluorescence in channel 1
	CH2 R	Relative fluorescence in channel 2
	CH3 R	Relative fluorescence in channel 3
	CH1 I/CH2 I	Fluorescence intensity in CH 1 / Fluorescence intensity in CH2
	CH2 I/CH3 I	Fluorescence intensity in CH 2 / Fluorescence intensity in CH3
	CH1 I/CH3 I	Fluorescence intensity in CH 1 / Fluorescence intensity in CH3

#220276 - $15.00 USD Received 6 Aug 2014; revised 17 Oct 2014; accepted 21 Oct 2014; published 7 Jan 2015

Table 4. P-value results from two-tailed Student's t-test, for all ROI. A p-value < 0.05 was considered to be significant.

	Index	RV	LV posterior	Border zone	LV anterior
Channel 1	τ	0.3407	0.0748	0.0078	< 0.0001
Channel 2	τ_{mean}	0.7680	0.1343	0.0115	< 0.0001
	τ_1	0.2271	0.3131	0.0214	< 0.0001
	τ_2	0.2110	0.0054	0.0038	< 0.0001
	β	0.4198	0.0728	0.0706	< 0.0001
Channel 3	τ_{mean}	0.6285	0.3961	0.0167	< 0.0001
	τ_1	0.1669	0.0753	0.0349	0.0003
	τ_2	0.2748	0.0185	0.0051	< 0.0001
	β	0.4914	0.0440	0.2795	< 0.0001
Channel 4	τ_{mean}	0.7391	0.5037	0.0107	< 0.0001
	τ_1	0.0196	0.0002	0.3874	0.0324
	τ_2	0.3773	0.5405	0.0099	< 0.0001
	β	0.0123	0.0180	0.2994	0.0004
	CH1 R	0.0021	0.0451	0.0172	< 0.0001
	CH2 R	0.0055	0.0041	0.0162	< 0.0001
	CH3 R	0.0016	0.0025	0.0073	< 0.0001
	CH1 I/ CH2 I	0.0007	0.0212	0.0040	< 0.0001
	CH2 I/ CH3 I	0.0034	0.0013	0.0072	< 0.0001
	CH1 I/ CH3 I	0.0061	0.0330	0.0271	< 0.0001

Cohen's d

Cohen's *d* is an appropriate effect size measurement for the comparison between two means. It indicates the standardized difference between two means, and expresses this difference in standard deviation units. The Cohen's *d* coefficient can be defined in terms of population means μ and standard deviations *s*, as shown below:

$$d = \frac{|\mu_1 - \mu_2|}{\sigma} \tag{A1}$$

where

$$\sigma = \sqrt{\frac{s_1^{\,2} + s_2^{\,2}}{2}} \tag{A2}$$

As an effect size measure, a larger Cohen's *d* represents a greater differentiation between two groups. Thus, it is traditionally presented as complementary to the report of results from a statistical significance test. Whereas the latter is used to suggest whether a difference exists between two groups, the Cohen's *d* reports the magnitude of this difference.

#220276 - $15.00 USD Received 6 Aug 2014; revised 17 Oct 2014; accepted 21 Oct 2014; published 7 Jan 2015

Table 5. Fluorescence parameters ranked by Cohen's d coefficient.

RV		LV posterior		Border zone		LV anterior	
Parameter	**Cohen's d**	**Parameter**	**Cohen's d**	**Parameter**	**Cohen's d**	**Parameter**	**Cohen's d**
CH1 I/CH2 I	2.8036	CH4 τ_1	3.2132	CH2 τ_2	2.1595	CH2 τ_2	13.4927
CH3 R	2.4672	CH2 I/CH3 I	2.5538	CH1 I/CH2 I	2.1435	CH3 τ_2	11.2469
CH1 R	2.3745	CH3 R	2.3114	CH3 τ_2	2.0612	CH2 τ	10.9477
CH2 I/CH3 I	2.2016	CH2 R	2.1350	CH2 I/CH3 I	1.9414	CH4 τ	9.7707
CH1 I/CH3 I	1.9966	CH2 τ_2	2.0432	CH3 R	1.9385	CH3 τ	9.5738
CH2 R	2.0333	CH4 β	1.6309	CH1 τ	1.9126	CH4 τ_2	9.1585
CH4 β	1.7603	CH3 τ_2	1.6215	CH4 τ_2	1.8327	CH2 β	8.8652
CH4 τ_1	1.6019	CH1 I/CH2 I	1.5762	CH4 τ	1.8066	CH3 R	7.6861
CH3 τ_1	0.8607	CH1 I/CH3 I	1.4274	CH2 τ	1.7817	CH1 τ	7.4315
CH2 τ_2	0.7717	CH3 β	1.3301	CH2 I	1.6671	CH2 I/CH3 I	6.8895
CH2 τ_1	0.7430	CH1 R	1.3214	CH3 τ	1.6558	CH3 β	6.0840
CH3 τ_2	0.6670	CH2 β	1.1575	CH1 R	1.6471	CH1 R	5.8111
CH1 τ	0.5776	CH1 τ	1.1483	CH2 τ_1	1.5728	CH2 R	5.5292
CH4 τ_2	0.5334	CH3 τ_1	1.1457	CH1 I/CH3 I	1.4936	CH1 I/CH2 I	5.4861
CH2 β	0.4857	CH2 τ	0.9408	CH3 τ_1	1.4084	CH1 I/CH3 I	4.7944
CH3 β	0.4124	CH2 τ_1	0.6133	CH2 β	1.1683	CH2 τ_1	4.1752
CH3 τ	0.2881	CH3 τ	0.5119	CH3 β	0.6602	CH3 τ_1	3.1062
CH4 τ	0.1977	CH4 τ	0.4005	CH4 β	0.6318	CH4 β	2.9804
CH2 τ	0.1750	CH4 τ_2	0.3659	CH4 τ_1	0.5217	CH4 τ_1	1.4332

Acknowledgments

This research was funded by the UK Engineering and Physical Sciences Research Council (EPSRC, grant reference: EP/I02770X/1). MBS is supported by the Wellcome Trust (WT092852). ARL is supported by a BHF Intermediate Research Fellowship FS/11/67/28954 and the NIHR Cardiovascular Biomedical Research Unit, Royal Brompton Hospital. We would like to acknowledge the ElectroCardioMaths Programme of the BHF Centre and RG/10/11/28457, and the Imperial NIHR BRC.